Supporting Information for

Aerosol trends dominate over global warming-induced cloud feedback in driving recent changes in marine low clouds

Yang Cao[1,2,†], Hao Wang[1,2,†], Yannian Zhu[1,2,*], Minghuai Wang[1,2*], Daniel Rosenfeld[1,3], Chen Zhou[1,2], Zhonghua Zheng[4], Hugh Coe[4], David Topping[4], Jihu Liu[1,2], Kang-En Huang[1,2], Yuan Liang[5], Haipeng Zhang[6,7], Heming Bai[8], Man Yue[9]

[1]School of Atmospheric Sciences, Nanjing University, 210023 Nanjing, China

[2]Joint International Research Laboratory of Atmospheric and Earth System Sciences & Institute for Climate and Global Change Research, Nanjing University, China

[3]Institute of Earth Sciences, The Hebrew University of Jerusalem, Jerusalem 91904, Israel

[4]Department of Earth and Environmental Sciences, The University of Manchester, Manchester M13 9PL, UK

[5]TianJi Weather Science and Technology Company, Beijing, China
[6]Department of Atmospheric and Oceanic Science, University of Maryland, College Park, MD, USA
[7]Earth System Science Interdisciplinary Center, University of Maryland, College Park, MD, USA

[8]Research Center for Intelligent Information Technology, Nantong University, China

[9]Zhejiang Institute of Meteorological Sciences, Hangzhou, China

Corresponding author: Yannian Zhu (yannian.zhu@nju.edu.cn) and Minghuai Wang (minghuai.wang@nju.edu.cn). †These authors contributed equally to this work.

Contents of this file

Text S1.
Figures S1-S8.

Text S1.

We estimated the contributions of ACI and cloud feedback to CRE trends through their impacts on cloud fraction and albedo based on the sensitivities of cloud properties to N_d and SST. The sensitivity of low-cloud properties to N_d was estimated using the deep learning model combined with a parameter perturbation method, as derived from our previous work (Cao et al., 2025, submitted). In contrast, the sensitivity of low-cloud properties to SST was calculated using a linear regression approach (Figure S5). The respective contributions of CF cloud albedo to CRE changes were then determined based on their relative proportions of CF and cloud albedo susceptibility to N_d/SST.

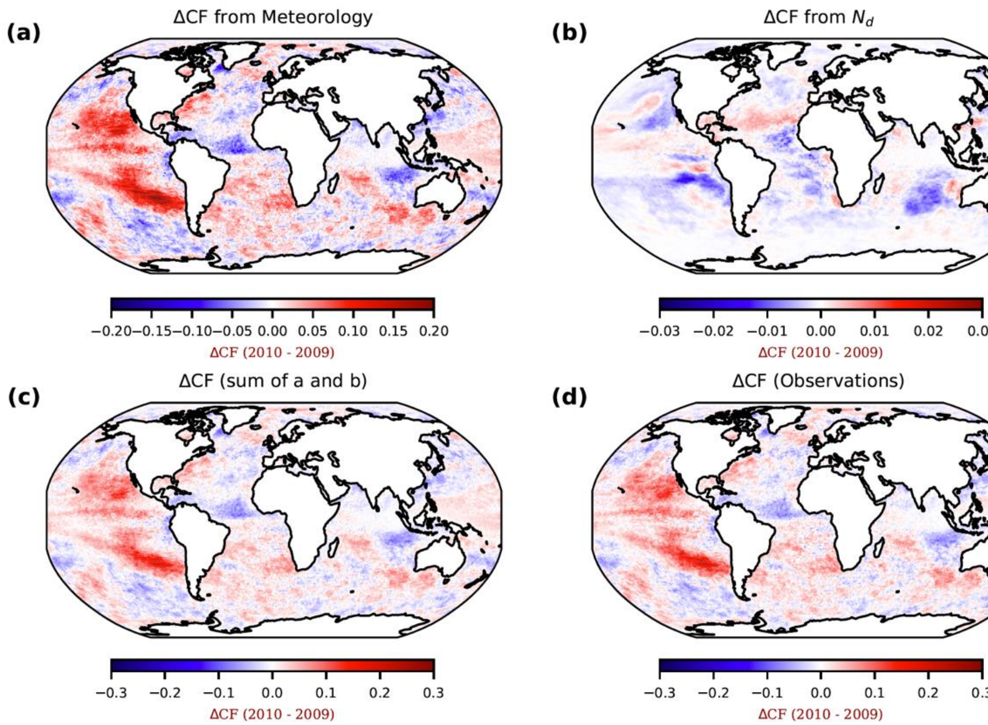

Figure S1. $CNN_{Met\text{-}Nd}$ separates the impacts of ENSO-related changes and N_d variations on CF. Panels (a) and (b) illustrate the contributions of meteorological factors and $\ln(N_d)$ to CF, respectively. Panel (c) shows the combined effect, representing the sum of panels (a) and (b). Panel (d) depicts the observed difference in low-cloud CF between 2010 and 2009.

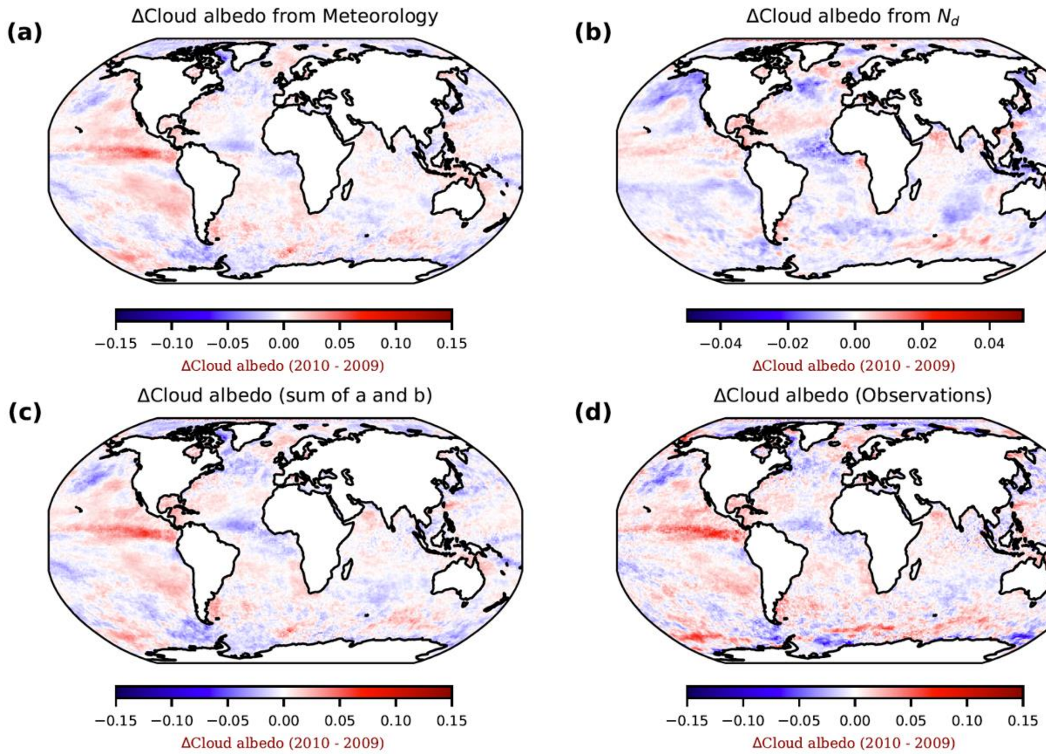

Figure S2. $CNN_{Met\text{-}Nd}$ separates the impacts of ENSO-related changes and N_d variations on cloud albedo. Panels (a) and (b) illustrate the contributions of meteorological factors and $\ln(N_d)$ to cloud albedo, respectively. Panel (c) shows the combined effect, representing the sum of panels (a) and (b). Panel (d) depicts the observed difference in low-cloud cloud albedo between 2010 and 2009.

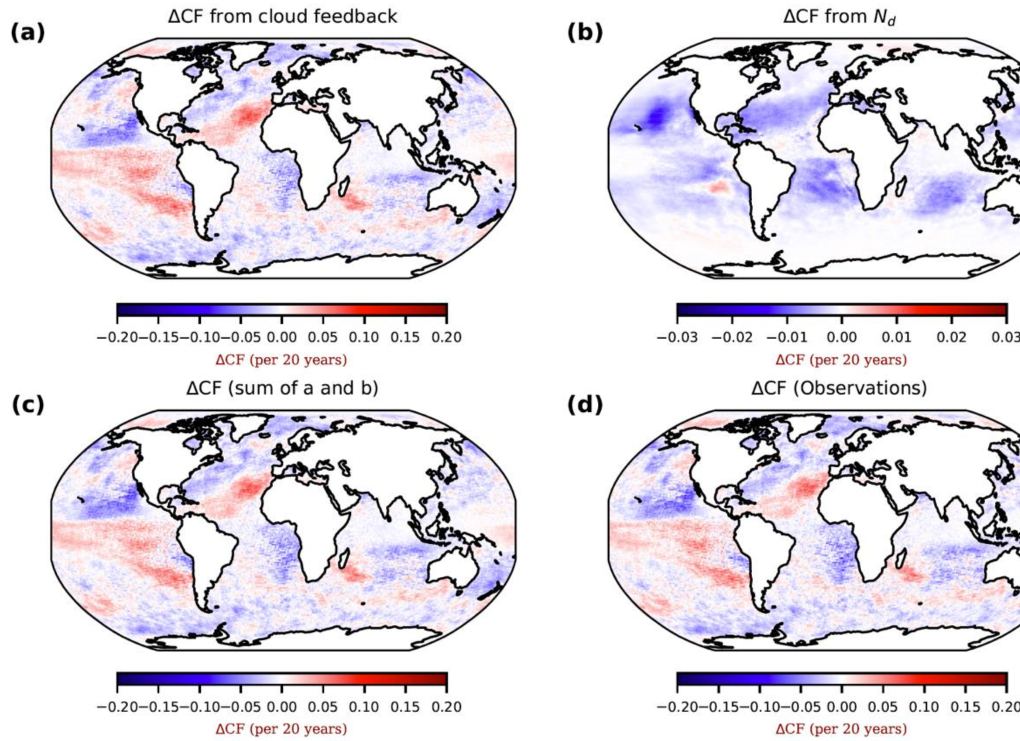

Figure S3. Spatial distribution of the effects of cloud feedback and aerosol-cloud interactions (ACI, through N_d) on CF trend changes from 2003 to 2022, as derived from the deep learning approach. Panels (a) and (b) illustrate the contributions of cloud feedback and ACI to changes in low-cloud CF. Panel (c) shows the combined effect, calculated as the sum of panels (a) and (b). Panel (d) presents the observed trend in CF based on CERES data for 2003–2022.

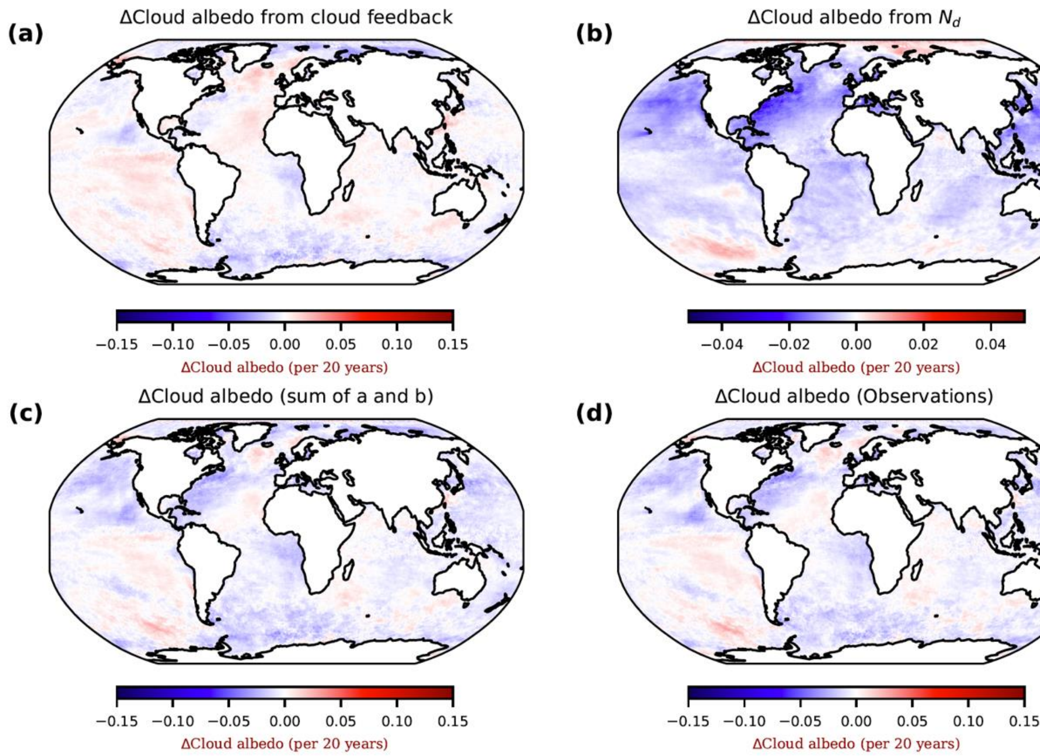

Figure S4. Spatial distribution of the effects of cloud feedback and ACI (through N_d) on cloud albedo trend changes from 2003 to 2022, as derived from the deep learning approach. Panels (a) and (b) illustrate the contributions of cloud feedback and ACI to changes in cloud albedo. Panel (c) shows the combined effect, calculated as the sum of panels (a) and (b). Panel (d) presents the observed trend in cloud albedo based on CERES data for 2003–2022.

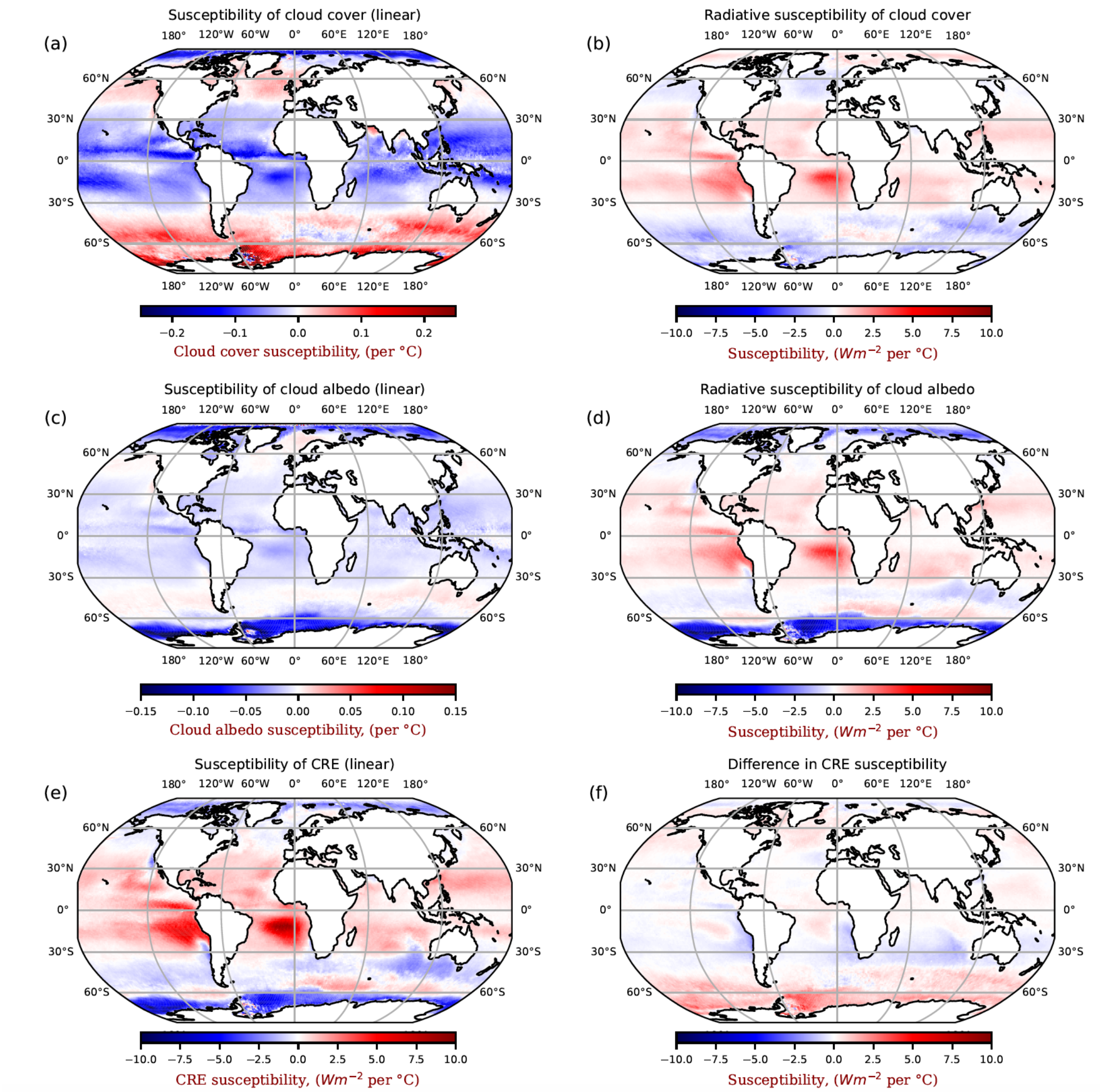

Figure S5. Spatial distribution of decomposed cloud susceptibility to SST. Panel (a) illustrates cloud cover (CC) susceptibility to SST, denoted as $\frac{\partial \mathrm{CC}}{\partial \mathrm{SST}}$. Panel (b) presents the radiative susceptibility of cloud cover to SST, expressed as $\overline{(A_{clr} - A_{cld})}(\frac{dCC}{\partial \mathrm{SST}})\overline{F^{\downarrow}}$. Aclr is the clear-sky albedo and $F^{\downarrow}$ is the incoming solar radiation. Panel (c) displays cloud albedo (Acld) susceptibility to SST, indicated by $\frac{\partial \mathrm{Acld}}{\partial \mathrm{SST}}$. Panel (d) shows the radiative susceptibility of cloud albedo to SST, represented as $\overline{CC}\left(\frac{dA_{clr}}{\partial \mathrm{SST}} - \frac{dA_{cld}}{\partial \mathrm{SST}}\right)\overline{F^{\downarrow}}$. Panel (e) depicts the CRE susceptibility to SST, denoted by $\frac{\partial \mathrm{CRE}}{\partial \mathrm{SST}}$. Finally, panel (f) illustrates the difference in CRE susceptibility to SST, calculated as the sum of panels (b) and (d) minus panel (e). The scale factor for each grid is derived by dividing Figures S6b and S6d by their sum.

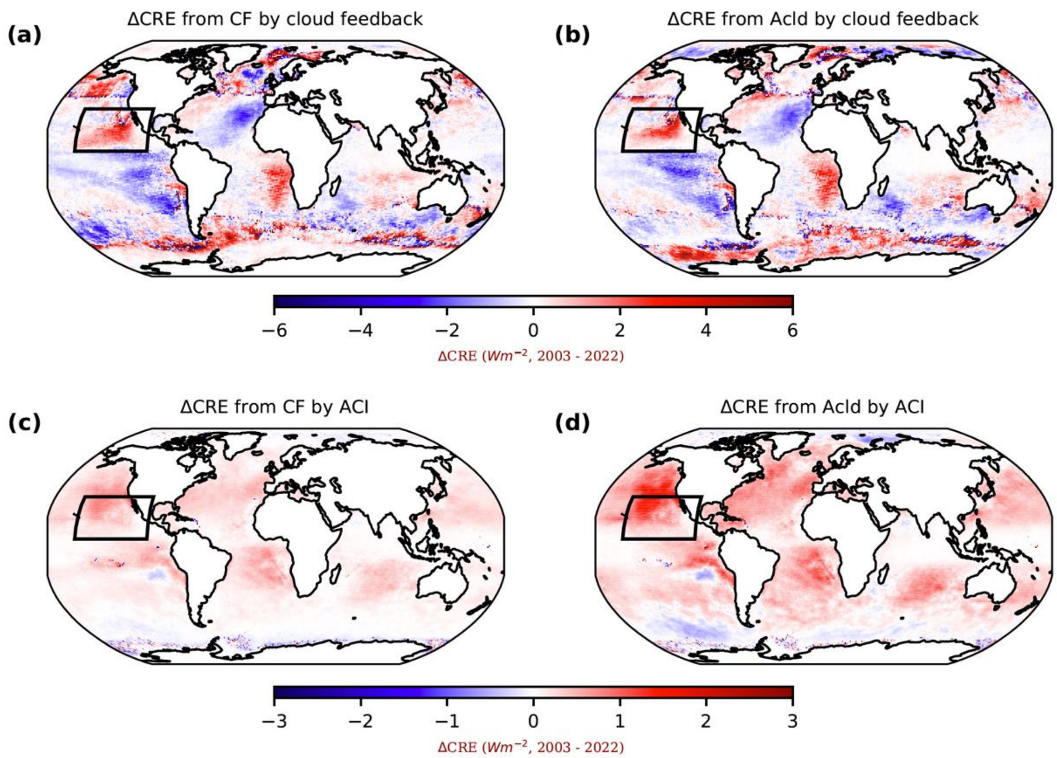

Figure S6. The spatial distribution of ΔCRE from 2003 to 2022 due to CF and cloud albedo (Acld) influenced by cloud feedback and ACI. Panels a and b illustrate the ΔCRE driven by cloud feedback, which affect both CF and Acld. In contrast, panels c and d present the ΔCRE induced by ACI, achieved by adjusting CF and Acld.

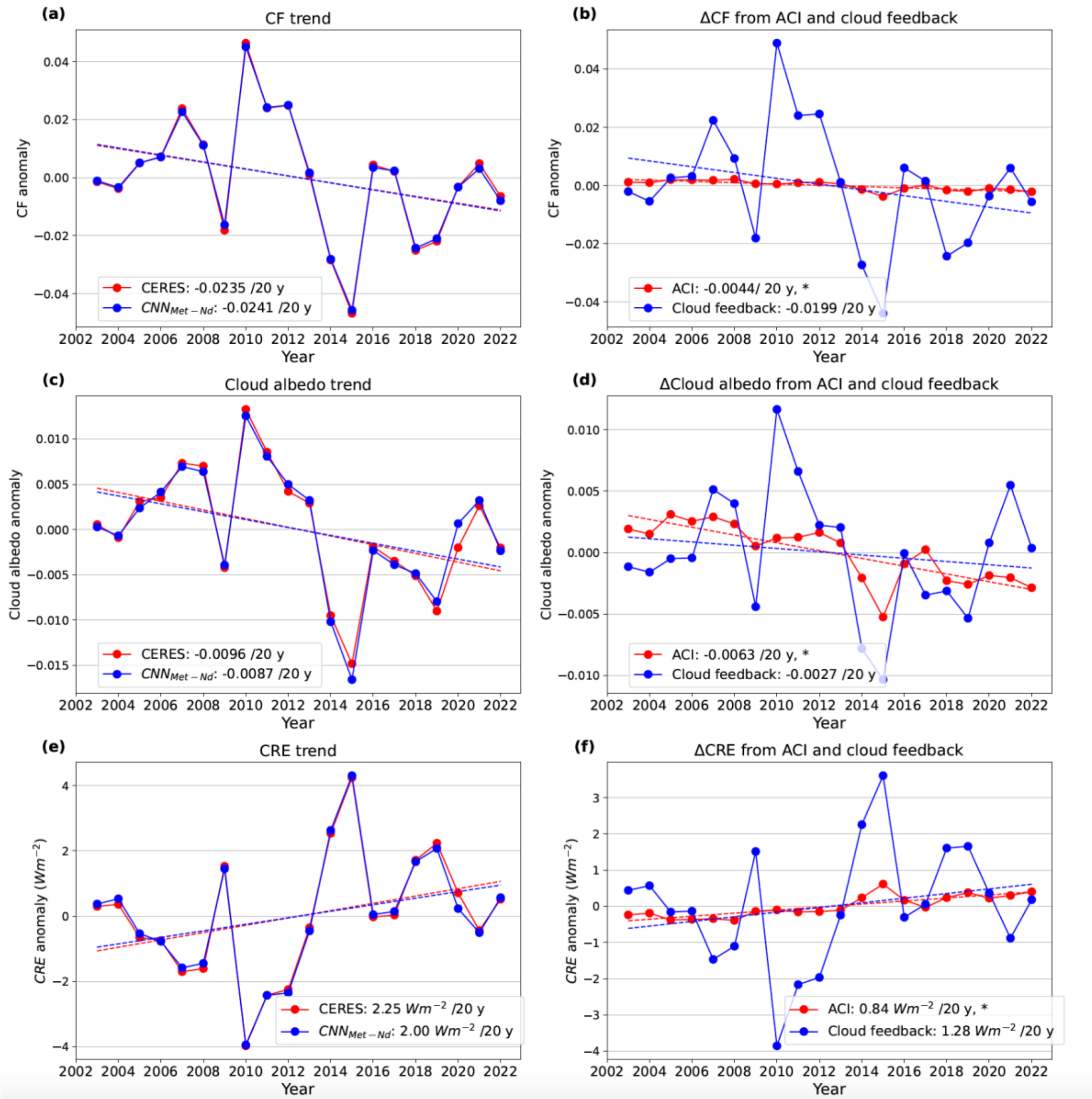

Figure S7. Time series of annual mean properties of marine low clouds from observations and predictions over the Northeastern Pacific (Figure S6). The left column represents cloud properties from observations and predictions of the deep learning model. The right column represents cloud changes induced by N_d and meteorology.

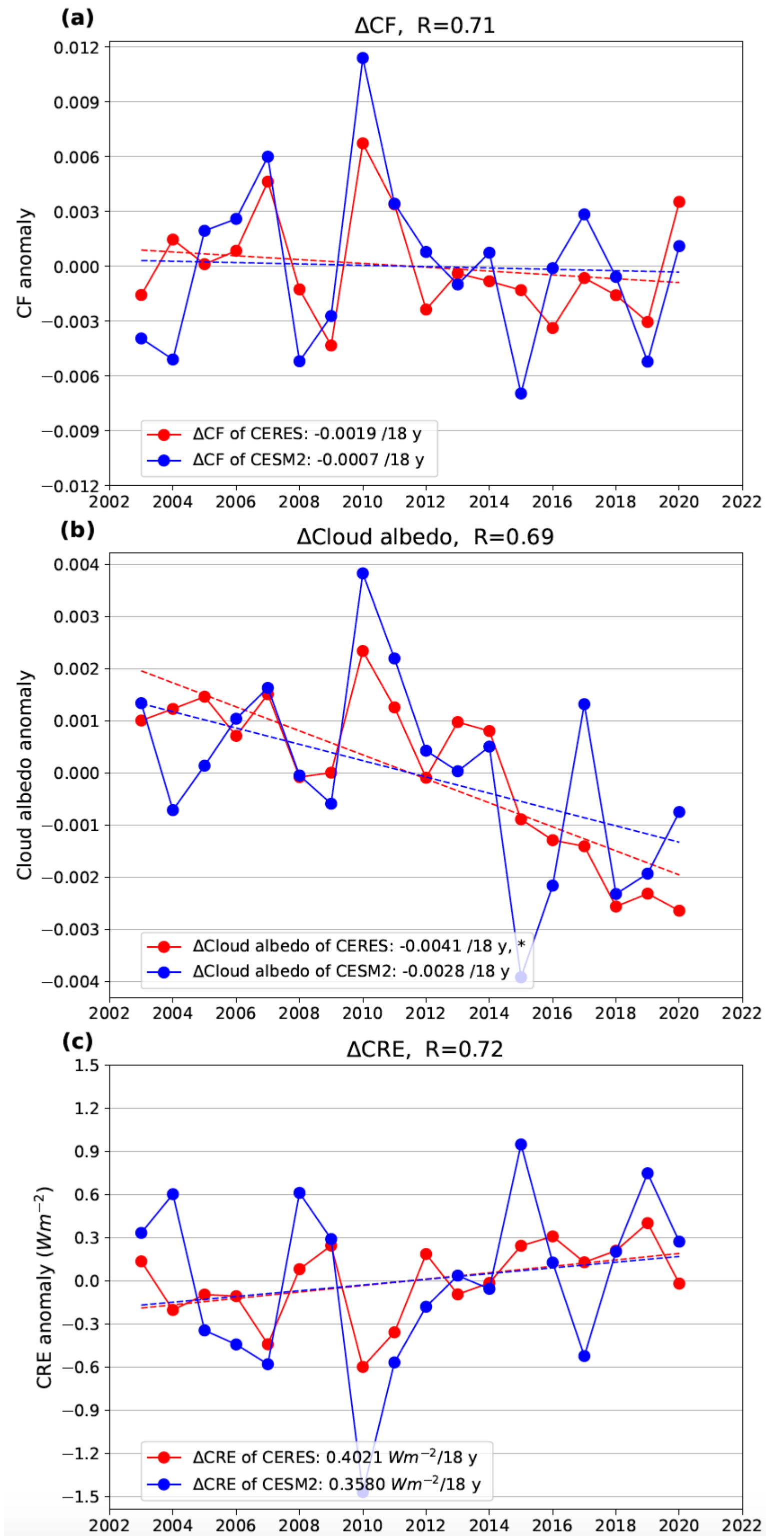

Figure S8. Time series of observed and simulated cloud properties from CERES and CESM2 for the period 2003–2020. An asterisk in the legend denotes results that meet the 95% significance level. The correlation coefficient (R) quantifies the relationship between the red and blue lines.

Reference

Cao et al., Quantifying Nonlinear Cloud Susceptibility and Radiative Forcing from Aerosol-Cloud Interactions Using Deep Learning.